Monte Carlo-fluid model of chlorine atom production in Cl_2, HCl, and CCl_4 radio-frequency discharges for plasma etching

Timothy J. Sommerer[a] and Mark J. Kushner[b]
University of Illinois, Department of Electrical and Computer Engineering, 1406 W. Green St., Urbana, Illinois 61801

(Received 21 April 1992; accepted 2 July 1992)

Chlorine chemistries are often used for the radio-frequency (rf) discharge plasma etching of compound semiconductors, metals, and silicon. A variety of gas mixtures are used as Cl atom donors, many of which have different electron transport coefficients. In this article we computationally investigate 13.56 MHz rf discharges sustained in He/Cl_2, He/HCl, and He/CCl_4 gas mixtures in the context of plasma etching. The study is performed using a Monte Carlo-fluid hybrid model of rf discharges. We find that the Cl atom production efficiency is surprisingly similar in these mixtures, while the details of the electron transport (sources of ionization, locations of attachment, electronegativity) dramatically differ. We also find that even at the low pressures of interest (0.25–1 Torr) attachment in He/HCl mixtures is dominated by vibrationally excited HCl, in analogy to high-pressure discharge devices.

I. INTRODUCTION

Chlorine chemistries are often used for the plasma etching of III–V semiconductors, Al, *n*-type Si, and polycrystalline silicon.[1] The etching precursor for these discharges is believed to be chlorine atoms. A variety of different gases are commonly used as Cl donors. Some examples of these donors are HCl, Cl_2, CCl_2F_2, $SiCl_4$, and CCl_4. The electron and ion transport coefficients for these gases are quite different. As a result, there is no expectation that the discharge properties (i.e., electron density, electronegativity, plasma potential) obtained using different Cl donors will be similar even though the etching rates may be similar. Likewise, similar power depositions and gas pressures do not necessary result in the same rate of Cl atom production. Since the etching characteristics of the discharge depend both on the rate of Cl production and parameters such as ion fluxes, some care must be taken in selecting the Cl donor for the etching conditions of interest.

A number of theoretical studies have addressed the properties of Cl_2 radio-frequency (rf) discharges. Rogoff, Kramer, and Piejak[2] computationally and experimentally investigated the bulk plasma in 13.56 MHz rf chlorine discharges. They found that the highly electronegative nature of the plasma resulted in power deposition which increased linearly with increasing electrode spacing (1.0–2.5 cm), current and gas pressure (1.0–1.5 Torr). These characteristics imply that the bulk plasma is well represented by a positive column in which ionization is balanced by attachment. Meyyappan and Govindan[3] modeled a Cl_2 rf discharge (13.56 MHz) using a three-moment fluid model. For an electrode separation of 1 cm and applied rf amplitude of 140 V, they obtained an ion density of $\simeq 2\times 10^{11}$ cm^{-3} and an electronegativity (negative ion density/electron density) of $\geqslant 100$. Under these conditions, space charge neutrality is maintained by the positive and negative ions, with the electrons being somewhat decoupled. Meyyappan and Govindan therefore predict that the electrons will advect across the discharge under the influence of the applied electric field and reach a maximum value near the electrodes on alternating half-cycles. The electron temperature was predicted to have $\simeq 30\%$ modulation during the rf cycle, with a mean value of 2.6 eV. Park and Economou,[4] and Aydil and Economou[5] developed one- and two-dimensional fluid models for Cl_2 discharges to investigate etching uniformities, and separately a bulk plasma model using a local field solution of the electron energy distribution to obtain rate coefficients. They also found electronegativities of $\simeq 100$ at a gas pressure of 1 Torr, and that electron densities modulated by $\simeq 15\%$ during the rf cycle.

In this article, we report on a computational investigation of rf discharges sustained in different chlorine donating gases as used for the etching of semiconductors. The goal of this study is to characterize the efficiency with which Cl atoms are produced, and how other properties of these discharges (such as electronegativity) compare. This study was performed with a self-consistent Monte Carlo-fluid (MCF) simulation for the electron, ion, and neutral kinetics in parallel plate rf discharges.[6] The gases investigated are HCl, CCl_4, and Cl_2. We found that the Cl atom production efficiency is highest for Cl_2 and lowest for HCl, and that the efficiency generally increases with increasing pressure and voltage, though the differences are not large. The dominant source of Cl atoms is dissociative electronic excitation in all cases, though dissociative ionization (for CCl_4 and Cl_2) and attachment may account for a few to 10% of the percent of the total Cl production. We also found that since the dissociative attachment cross section for HCl significantly increases with increasing vibrational level, HCl(v) must be accounted for in low pressure models of etching discharges.

In Sec. II, the model we used in this study will be briefly described and the results of our investigation are discussed in Sec. III. Our concluding remarks are in Sec. IV.

 ©1992 American Vacuum Society

II. DESCRIPTION OF THE MODEL

The model used in this study is a self-consistent Monte Carlo-fluid hybrid (MCFH) model for the electron, ion, and neutral kinetics in parallel plate rf discharges. The MCF simulation is discussed in detail in Ref. 6, and therefore will be only briefly described here.

The MCFH model consists of three linked simulations, an electron Monte Carlo simulation (EMCS), a self-consistent fluid model (SCFM), and a neutral chemistry and transport model (NCTM). In the EMCS, electron trajectories are calculated in an oscillating rf electric field while accounting for collisions with the input gases, ions, and other species which evolve during the simulation. The EMCS begins by assuming an electric field as a function of position between the electrodes and phase during the rf cycle, $E(z,\phi)$. This electric field is used to advance the electron trajectories for 10s of rf cycles to generate electron impact source functions, $S(z,\phi)$, for excitation, ionization, and dissociation of the gases, as a function of position and phase. Electron transport coefficients (mobility, average energy) are also produced in the EMCS. The $S(z,\phi)$ and transport coefficients are then transferred to the SCFM. In the SCFM the charge densities for electrons, positive ions, and negative ions are obtained from their respective continuity equations using the source functions and transport coefficients from the EMCS. $E(z,\phi)$ is obtained in the SCFM by solving Poisson's equation. All pertinent charged particle chemistry (e.g., Penning and charge exchange reactions) are included in this portion of the model. The SCFM is also run for 10s of rf cycles. At that time, the charge densities and $E(z,\phi)$ are returned to the EMCS. The EMCS is run for 10s of rf cycles using the new field, generating new source functions for use in a subsequent run of the SCFM. We continue to iterate between the EMCS and SCFM until the average plasma density converges to acceptable limits (see Ref. 6).

Before execution of the SCFM during each iteration, $S(z,\phi)$ and the charge densities may be transfered to the NCTM in which neutral radical and molecular densities are calculated. The resulting densities are then used in both the EMCS and SCFM. Typically, 100s to 1000s of rf cycles are required for the calculation to converge. This requires hours to 10s of hours on a laboratory computer (Stardent 3000).

The major revision to the model described in Ref. 6 is in the manner in which $S(z,\phi)$ is transferred to the SCFM. In highly attaching gas mixtures, small changes in the charge balance can cause large changes in $E(z,\phi)$ between iterations between the EMCS and SCFM. These changes in $E(z,\phi)$ are reflected in the source functions which are cycled back to the SCFM. The end result is an oscillation in the plasma density whose time scale corresponds to many ion diffusion times across the plasma. This phenomenon may require many 1000s of rf cycles to damp out. We feel this is a numerical effect since these low frequency oscillations are not typically observed experimentally.[7] This effect is largely mitigated by back averaging $S(z,\phi)$ between successive interations between the EMCS and the SCFM. This back averaging is performed by

TABLE I. Species included in the model.

He	Cl_2	HCl	CCl_4
He*	Cl^+	$HCl(v=1,2)$	CCl_3^+
He^+	Cl^-	HCl^+	CCl_2
e	Cl		

$$S'_{i+1}(z,\phi)=fS_{i+1}(z,\phi)+(1-f)S'_i(z,\phi), \quad (1)$$

where the subscript denotes the iteration, the primes denote the back-averaged values, and the unprimed quantities are the raw instantaneous values. For highly attaching mixtures, we used $f=0.5$. We also revised the manner of recording particle locations in the EMCS. In this work we recorded particle locations in phase space (position, rf phase, energy) every time a particle's trajectory was updated. Since the time steps used to advance individual particles differ, the recording of each particle's position in a given cell of phase space is weighted by the length of the previous timestep or the length of time spent in that cell, whichever is shorter.

Cross sections for attachment, vibrational excitation, electronic excitation, and momentum transfer for CCl_4 were obtained from Hayashi.[8] Cross sections for dissociative ionization for CCl_4 were obtained from Leiter *et al.*[9] In accordance with Hayashi,[8] and Breibarth and Rottmayer,[10] we assumed that all electronic excitations are dissociative. A single branching to CCl_2+2Cl was used, as suggested by Breibarth and Rottmayer.[10] Cross sections for all processes in Cl_2 were obtained from Rogoff *et al.*[2] Electronic excitation to the $C\,^1\Pi$ state of Cl_2 is dissociative. Cross sections for momentum transfer, electronic excitation and ionization of HCl were obtained from Hayashi.[8] Cross sections for vibrational excitation to $HCl(v=1,2,3)$ were obtained from Penetrante and Bardsley,[11] and cross sections for dissociative attachment to $HCl(v=0,1,2,3)$ were obtained from Bardsley and Wadhera.[12] Electron superelastic quenching cross sections for all levels were calculated by detailed balance. We approximated that the electronic excitation and ionization cross sections for $HCl(v=0)$ could be used for $HCl(v>0)$ by decreasing their threshold values by the vibrational quanta.

Helium is a common diluent used in etching of semiconductors, and so the gas mixtures used in this study were $He/M=0.9/0.1$, $M=CCl_4$, HCl, and Cl_2. The species included in the model are listed in Table I. The electron impact and heavy particle reactions included in the model for these mixtures are shown in Table II.

The attachment cross sections of the feedstock gases dramatically vary, as shown in Fig. 1. CCl_4 has a large thermal attachment cross section. The cross section for dissociative attachment to Cl_2 also has a thermal component, though 50–100 times smaller than CCl_4. There are small resonances in the Cl_2 attachment cross section between 1 and 10 eV, though these resonances do not significantly contribute to the total Cl_2 attachment.

The attachment cross section for $HCl(v=0)$ is, in comparison, small and has a threshold energy of 0.75 eV. The attachment cross section, though, increases with increasing

TABLE II. Reactions included in the model.

Process	Rate coefficient[a]	Reference
All gas mixtures		
$e+He \rightarrow He+e$	b	13
$e+He \rightleftarrows He^{*}+e$	b,c	14
$e+He \rightleftarrows He^{**}+e$	b,c	14
$e+He \rightarrow He^{+}+2e$	b	15
$e+He^{*} \rightarrow He^{+}+2e$	b,c	16
$e+He^{*} \rightleftarrows He^{**}+e$	b,c	17
$e+He^{**} \rightarrow He^{+}+2e$	b,c	16
$e+He^{+} \rightarrow He^{+}+e$	b	18
$He^{*}+He^{*} \rightarrow He^{+}+He+e$	1.5×10^{-9}	19
$He^{*}+He \rightarrow 2He$	5.8×10^{-15}	20
$e+Cl^{-} \rightarrow Cl^{-}+e$	b	18
$e+Cl^{-} \rightarrow Cl+e$	b	21
$Cl^{-}+He^{+} \rightarrow Cl+He$	5.0×10^{-8}	d
Additional reactions for He/Cl_2		
$e+Cl_2 \rightarrow Cl_2+e$	b	2
$e+Cl_2 \rightarrow Cl_2(v=1,2,3)+e$	b	2
$e+Cl_2 \rightarrow Cl_2(B\,^3\Pi,2\,^1\Pi,2^1\Sigma)+e$	b	2
$e+Cl_2 \rightarrow Cl_2(C\,^1\Pi)+e \rightarrow 2Cl+e$	b	2
$e+Cl_2 \rightarrow Cl_2^{+}+2e$	b	2
$e+Cl_2 \rightarrow Cl^{-}+Cl$	b	2
$e+Cl_2^{+} \rightarrow Cl+Cl$	b	d,22
$e+Cl_2^{+} \rightarrow Cl_2^{+}+e$	b	18
$He^{*}+Cl_2 \rightarrow Cl_2^{+}+He+e$	1.0×10^{-10}	d
$He^{+}+Cl_2 \rightarrow Cl_2^{+}+He$	1.0×10^{-9}	d
$Cl_2^{+}+Cl^{-} \rightarrow 3Cl$	5.0×10^{-8}	d
Additional reactions for He/HCl		
$e+HCl(v=0,1,2) \rightarrow HCl(v=0,1,2)+e$	b,e	8
$e+HCl \rightleftarrows HCl(v=1,2)+e$	b	11
$e+HCl(v=1) \rightleftarrows HCl(v=2)+e$	b	11
$e+HCl(v=0,1,2) \rightarrow H+Cl+e$	b,e	8
$e+HCl(v=0,1,2) \rightarrow HCl^{+}+2e$	b,e	8
$e+HCl(v=0,1,2) \rightarrow H+Cl^{-}$	b	12
$e+HCl^{+} \rightarrow H+Cl$	b	d,22
$e+HCl^{+} \rightarrow HCl^{+}+e$	b	18
$HCl^{+}+Cl^{-} \rightarrow H+2Cl$	5.0×10^{-8}	d
$HCl(v=1)+HCl \rightarrow 2HCl$	2.18×10^{-14}	23
$HCl(v=2)+HCl \rightarrow HCl+HCl(v=1)$	4.35×10^{-14}	23
$HCl(v=1)+HCl(v=1) \rightarrow HCl(v=2)+HCl$	3.0×10^{-12}	23
$He^{*}+HCl(v=0,1,2) \rightarrow HCl^{+}+He+e$	1.0×10^{-10}	d
$He^{+}+HCl(v=0,1,2) \rightarrow HCl^{+}+He$	1.0×10^{-9}	d
Additional reactions for He/CCl_4		
$e+CCl_4 \rightarrow CCl_4+e$	b	8
$e+CCl_4 \rightarrow CCl_4(v=1,2,3)+e$	b	8
$e+CCl_4 \rightarrow CCl_2+2Cl+e$	b	8,10
$e+CCl_4 \rightarrow CCl_3^{+}+Cl+2e$	b,f	9
$e+CCl_4 \rightarrow CCl_3+Cl^{-}$	b	8
$e+CCl_3^{+} \rightarrow CCl_2+Cl$	b	d,22
$e+CCl_3^{+} \rightarrow CCl_3^{+}+e$	b	18
$CCl_3^{+}+Cl^{-} \rightarrow CCl_2+2Cl$	5.0×10^{-8}	d
$He^{*}+CCl_4 \rightarrow CCl_3^{+}+Cl+He+e$	1.0×10^{-10}	d
$He^{+}+CCl_4 \rightarrow CCl_3^{+}+Cl+He$	1.0×10^{-9}	d

[a]Rate coefficient has units $cm^3\ s^{-1}$ unless otherwise noted.
[b]Rate coefficient obtained from calculated electron energy distribution and cross section obtained from noted reference.
[c]He* represents a composite state. See Ref. 6.
[d]Estimated. See reference for analogous process.
[e]Cross sections for electron collisions for HCl($v=0$) were also used for HCl($v=1,2$), with the threshold energy appropriately modified.
[f]All dissociative ionization branchings for CCl_4 were summed and represented by a single branching to CCl_3^{+} in the model.

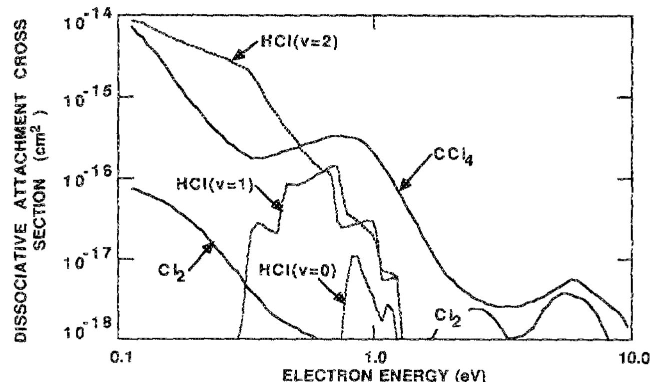

FIG. 1. Dissociative attachment cross sections for Cl_2, CCl_4, and HCl(v). Note the large thermal attachment cross section for CCl_4, and the large vibrational enhancement in the cross section for HCl(v).

vibrational level while the threshold energy decreases. As we will discuss below, even in the low pressure discharges of interest, attachment processes in HCl plasmas are dominated by the vibrationally excited species. This is a well-known phenomenon in high-pressure discharges containing HCl, such as those used in XeCl excimer lasers.[24] Although there is some expectation that $CCl_4(v)$ and $Cl_2(v)$ may also have larger attachment cross sections, the fractional increase in the total rate of attachment due to vibrationally enhanced attachment will be small due to the thermal attaching nature of the ground state.

III. CHARACTERISTICS OF rf DISCHARGES IN Cl DONORS

In this section, we will discuss characteristics of 13.56 MHz parallel plate rf discharges sustained in He/M=0.9/0.1, M=Cl_2, CCl_4, and HCl. Unless otherwise noted, the gas pressure is 250 mTorr, and the electrode separation is 2.54 cm (1 in.). The applied voltages specified below are rf amplitudes. We note that gas flow and depletion of feedstock gases are not included in this model.

The time averaged electric fields for He/Cl_2 mixtures are shown in Fig. 2. Electric fields are shown for applied potentials of 75, 100, and 150 V, and at pressures of 0.25, 0.5, and 1.0 Torr for 100 V. The thickness of the time averaged electric field is largely determined by the ion mean free path, which is a weak function of electric field. Therefore, as the voltage is increased, the thickness of the sheath remains nearly constant while the maximum electric field increases to account for the increase in voltage. The sheath thickness scales inversely with gas pressure to reflect the change in the ions' mean free path.

Time and spatially averaged electron densities and positive ion densities for Cl_2 discharges (0.25–1.0 Torr, 75–150 V) are shown in Fig. 3. Over the range of operating conditions studied, the plasma densities increase linearly with applied potential, but less than linearly with pressure. The positive ion density ($0.5–4\times10^{10}\ cm^{-3}$) is dominated by Cl_2^{+}. In spite of the larger mole fraction of He, the density of He^{+} is small ($10^{7}–10^{8}\ cm^{-3}$). The production of He^{+} is low and it is rapidly depleted by charge exchange

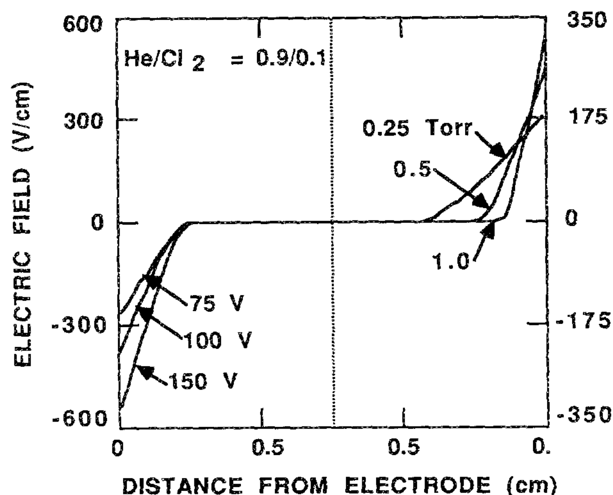

FIG. 2. Time averaged electric fields in $He/Cl_2=0.9/0.1$ mixtures for various rf voltages and gas pressures. The discharge is symmetric across the center line, and regions only 0.75 cm from the electrodes are shown. The varying voltage cases are at 0.5 Torr; the varying pressure cases are at 100 V. The sheath thickness is nominally only a function of pressure for these conditions.

with Cl_2. The electronegativity (negative ion density/electron density) is 15–20 at 0.25 Torr, increasing to 30–60 at 1 Torr. These values are somewhat lower than those predicted by Meyyappan[3] and Economou[4] for pure Cl_2 discharges. These values are a factor of 2–3 larger than densites for Cl_2^+ estimated from laser induced fluorescence (LIF) measurements by Donnelly, Flamm, and Collins for similar gas mixtures and power deposition (based on $W\,cm^{-2}$).[25] We attribute these differences to a possible depletion of the feedstock gases in the experiments, as noted by a saturation of ion density with increasing power, and a higher rate of loss of ions by radial diffusion in the relatively small experimental reactor (3.8 cm diam electrodes). Although numerous LIF experiments of ion densities and electric fields have been performed on attaching gases (see, for example, Ref. 26 and citations therein), the majority of those measurements have been in BCl_3 (for which electron collision cross sections are not available) or at lower rf frequencies. We can, however, compare to the experimental results of Gottscho[26] who measured sheath thickness in an Ar/BCl_3 (95/5, 0.3 Torr, 10 MHz) discharge. He found maximum sheath thicknesses of $\simeq 0.3$ cm, commensurate with those predicted here.

The average electron and positive ion densities in He/HCl discharges are shown in Fig. 3(c) for the same conditions as for He/Cl_2 in Fig. 3(b). For a given pressure and applied potential, the plasma density is approximately twice as large in the HCl discharge, and the electronegativity is smaller (10–15). This trend is largely a consequence of the rate of attachment to $HCl(v=0)$ being much smaller than that for Cl_2, and that HCl must be vibrationally excited to significantly attach. These trends are discussed in more detail below.

It is well-known from experience with atmospheric pressure discharges that attachment in HCl containing gas mixtures, such as for XeCl lasers, is dominated by vibrationally excited HCl.[24] To investigate this issue in low pressure, plasma processing discharges, calculations were performed including and excluding attachment to $HCl(v)$. The results for electron density are shown in Fig. 4(a) where the gas pressure is 0.25 Torr, and rf voltage is 100 V. The densities of ions are shown in Fig. 4(b). The densities of $HCl(v)$ and He* are shown in Fig. 5. When including $HCl(v)$, the electron density has a maximum value of

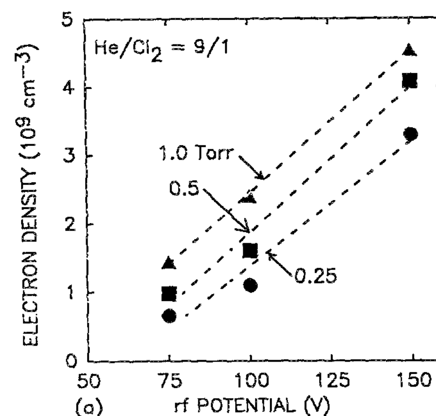

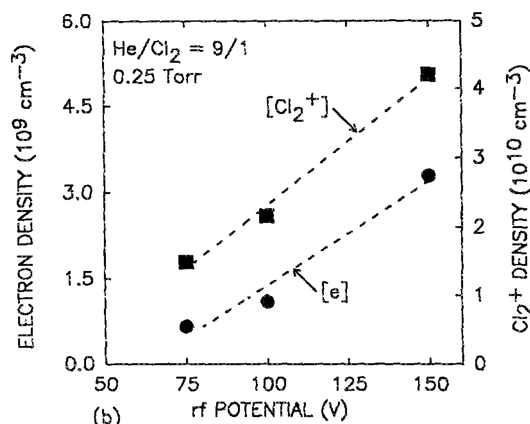

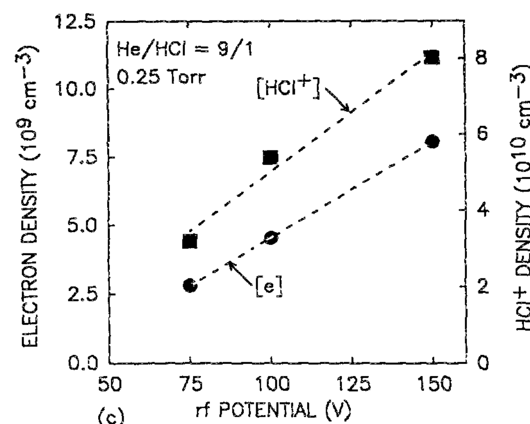

FIG. 3. Time and space averaged charge particle densities in He/Cl_2 and He/HCl gas mixtures. (a) Electron density as a function of rf voltage for various gas pressures for He/Cl_2. (b) Cl_2^+ and electron densities at 0.25 Torr as a function of rf voltage for He/Cl_2. (c) HCl^+ and electron densities at 0.25 Torr as a function of rf voltage for He/HCl. Plasma densities increase nearly linearly with voltage and less than linearly with pressure. For otherwise similar conditions, the plasma density is lower and electronegatively higher in He/Cl_2 mixtures.

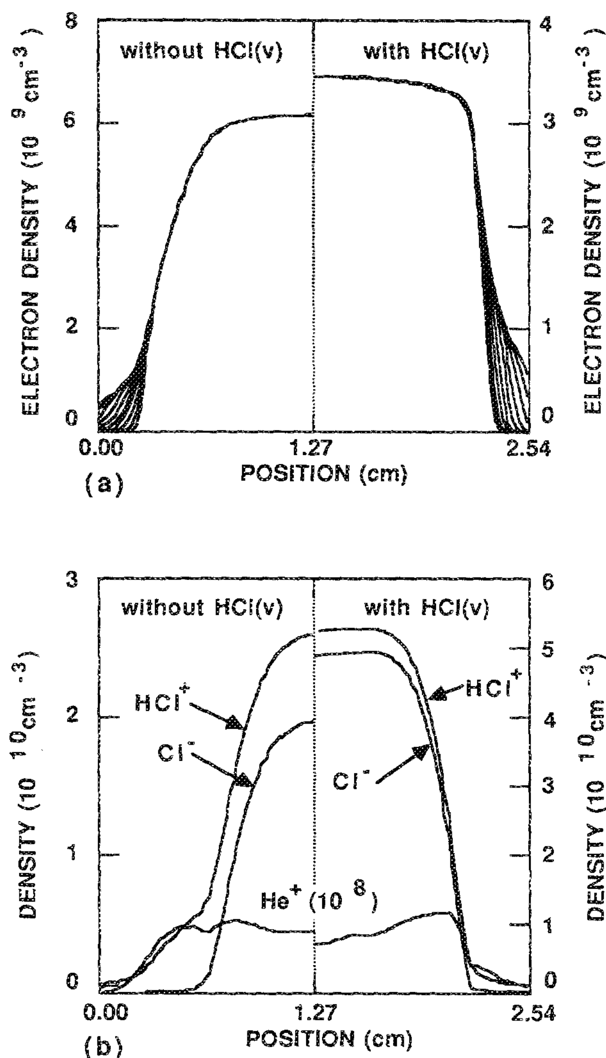

FIG. 4. Charged particle densities in He/HCl mixtures (0.25 Torr, 100 V) as a function of position when including and excluding vibrationally excited HCl. The results are symmetric across the center line. (a) Electron densities shown every 1/20 of the rf cycle for half the cycle. Without $HCl(v)$, the electron density is twice as large; with a profile which is more diffusion dominated. (b) Time averaged densities of HCl^+, Cl^-, and He^+. The positive and negative ion densities increase while the electron density decreases with $HCl(v)$, a consequence of increased rates of attachment.

3.5×10^9 cm^{-3}, compared to 6.2×10^9 cm^{-3} when excluding the vibrational states. The electronegativities for these two cases are 15 and 3, respectively. When including $HCl(v)$, the plasma density is more uniform across the plasma and the electron temperature is higher (2.1 eV compared to 1.8 eV), both characteristics of more electronegative plasmas. Note that the density of He^+ is $\simeq 500$ times smaller than HCl^+, a consequence of the He higher ionization potential and rapid rate of charge exchange. The densities of He^+ and He* are maximum near the edge of the sheaths where their rates of production are higher, but quickly decay due to charge exchange, Penning reactions, and to a lesser extent ion–ion neutralization. The peak densities of $HCl(v=1)$ and $HCl(v=2)$ are 3.9×10^{13} cm^{-3} and 1.5×10^{13} cm^{-3} at 100 V, yielding a total fractional density of HCl which is vibrationally excited of 0.07. The $HCl(v)$ densities increase somewhat linearly with increasing applied voltage, as shown in Fig. 5(b). As in excimer laser discharges,[24] moderate densities of $HCl(v)$ are sufficient to dominate attachment in HCl containing plasmas due to the large enhancement in their dissociative attachment cross sections relative to the ground state. Similar vibrational enhancements for attachment in H_2 have been exploited in the context of multicusp negative ion sources.[27]

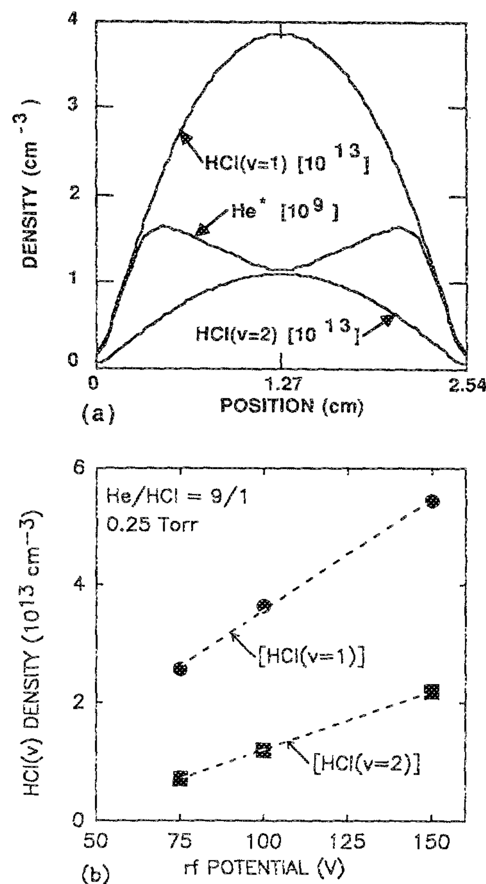

FIG. 5. Neutral particle densities in He/HCl discharges. (a) Time averaged HCl ($v=1,2$) and He* (0.25 Torr, 100 V) as a function of position between the electrodes. (b) Time and spatially averaged HCl ($v=1,2$) as a function of rf voltage at 0.25 Torr. The fractional densities of $HCl(v)$ are 5%–10%, while the density of He* is rapidly depleted by Penning reactions.

The electron sources (due to ionization, attachment, and recombination) are shown in Fig. 6 as a function of position and phase for rf discharges in $He/Cl_2=0.9/0.1$ at pressures of 0.25 and 1.0 Torr. The electric fields for these cases are shown in Fig. 6(c). The applied rf potential is 150 V. The contours which are not overlayed by dots denote regions in the (z,ϕ) phase space where ionization exceeds losses. The contours which are overlayed by dots denote regions where losses due to attachment and recombination exceed ionization. As expected, the lower pressure plasma is more nonequilibrium. Electrons are stochastically heated at the expanding front of the sheath, and penetrate further into the bulk plasma. This results in more

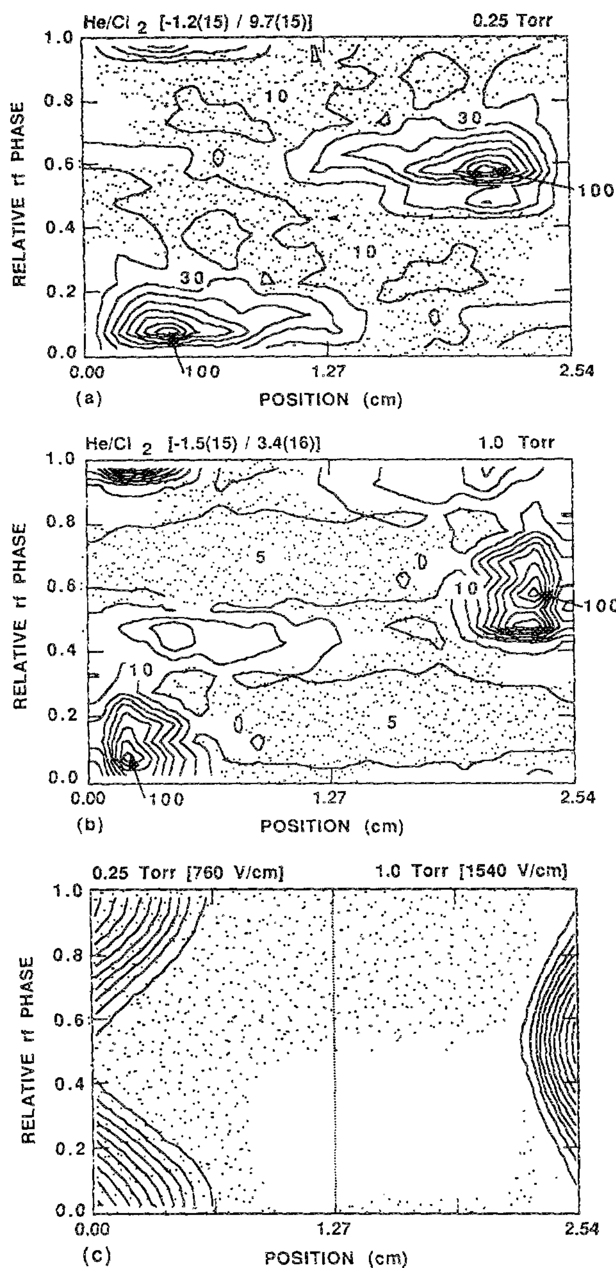

FIG. 6. He/Cl_2 electron sources and electric fields (150 V). (a) Electron sources by electron impact events (ionization, attachment, and recombination) as a function of position between the electrodes and phase during the rf cycle for 0.25 Torr. (b) Electron sources for 1.0 Torr. (c) Electric fields for 0.25 and 1.0 Torr. In (a) and (b) the contours not overlayed with dots denote regions of positive sources (that is, net ionization) while the contours overlayed with dots show regions of negative sources (that is, net loss). The contours are labeled as a percentage of their maximum values, separately shown at the top of each figure for losses and sources ($cm^{-3}\,s^{-1}$). In (c) the contours not overlayed with dots are positive fields and the contours overlayed with dots are negative fields. The maximum amplitude of the field is shown at the top of the figure.

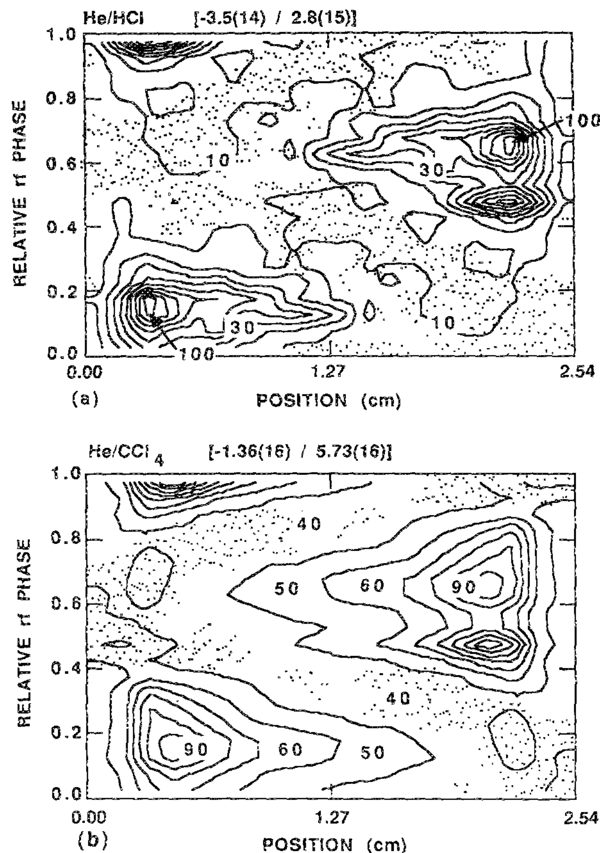

FIG. 7. Electron sources for (a) He/HCl (0.25 Torr, 75 V) and (b) He/CCl_4 (0.25 Torr, 600 V). The labeling scheme is the same as for Fig. 6.

widespread regions of net ionization. The losses are due dominantly to attachment and occur throughout the cycle. The maximum in the rate of loss in the bulk plasma is 10%–15% that of ionization. At 1.0 Torr, the regions of net ionization are confined to a smaller region of the (z,ϕ) phase space near the maximum extent of the sheaths. The electron losses have roughly the same magnitude and extent over (z,ϕ); hence the magnitude of the net ionization must increase to maintain the discharge. The electric field in the bulk plasma has maximum values of <2–$3\ V\ cm^{-1}$. There is evidence of an electric field reversal at higher pressures, as shown in Fig. 6(c), which is absent at the lower pressure.

The electron sources for He/HCl and He/CCl_4 discharges at 0.25 Torr are shown in Fig. 7. He/HCl discharges are able to operate in a similar pressure-voltage parameter space as He/Cl_2 discharges; and when HCl is vibrationally excited the rates of attachment in the He/Cl_2 and He/HCl plasmas are similar. Therefore, the magnitudes of the electron sources, and the regions of (z,ϕ) in which the sources have net ionization or loss, are similar. The situation in He/CCl_4 discharges, though, is quite different. The thermal attachment cross section for CCl_4 is more than 100 times greater than either Cl_2 or HCl, and this requires rf discharges in CCl_4 to operate at much higher voltages. The case shown in Fig. 7(b) is for a rf amplitude of 600 V. To generate similar total plasma densities (see below), the electron sources in He/CCl_4 have net rates of electron loss (by attachment) which are >10 times larger than for He/HCl or He/Cl_2, and also have commensurately larger rates of net ionization. The quasisteady state in the He/CCl_4 discharge is maintained by a balance between large sources and large rates of loss. Small

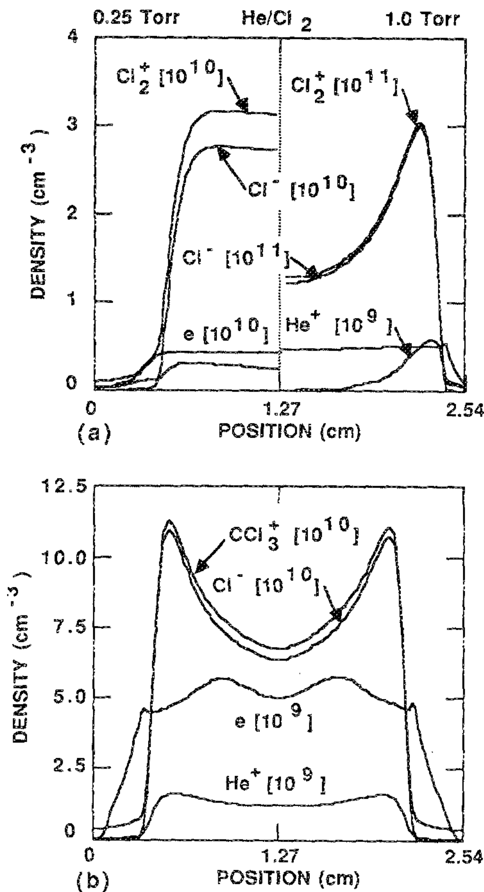

FIG. 8. Time averaged charged particle densities as a function of position between the electrodes. (a) He/Cl_2 for 0.25 and 1.0 Torr. (b) He/CCl_4 (0.25 Torr, 600 V). In all cases, ionization is maximum near the sheaths. Under conditions where the mean free path for loss is short, the ion densities are maximum near the sheath edge. This occurs at higher pressures in He/Cl_2 and low pressures in He/CCl_4 due to its high attachment cross section.

excursions from the operating point therefore lead to more rapid changes in discharge properties. This may explain the poor reproducibility and heightened sensitivity of highly attaching gas mixtures to small changes in operating conditions.

As is typical for rf discharges sustained in molecular gases, the maximum in the ionization rates are near the oscillating edges of the sheaths. The spatial distribution of charged species is then largely determined by their mean free path for loss by attachment, ion–ion recombination, recombination, or loss at the wall from their source of generation. For example, the spatial distribution of HCl^+ and Cl^- at 0.25 Torr [Fig. 4(b)] indicate production near the sheath edges with a moderate loss in the bulk plasma. The net flux of He^+ ions towards the center of the plasma indicates a net loss from charge exchange in the bulk. The spatial distributions of Cl_2^+, Cl^-, and He^+ in 0.25 Torr He/Cl_2, plotted in Fig. 8(a), show similar trends. However, in 1 Torr He/Cl_2 mixtures [also shown in Fig. 8(a)] the plasma densities are higher and ion mean free paths for loss are commensurately shorter. As a result, the ion densities are maximum near the sheath edge, with a net flux towards the center of the plasma compensated dominantly by ion–ion neutralization. The same phenomenon occurs in He/CCl_4 discharges at a lower pressure, as shown in Fig. 8(b), since the rates of attachment and ionization are commensturately larger. Note that there is a steady diffusion flux of positive and negative ions towards the center of the plasma. The rf current continuity is maintained by small modulating electric fields which balance the diffusion flux with an opposing drift. This condition is discussed in Ref. 6 in the context of electronegative O_2 discharges.

Cl atoms are believed to be the major etching species in the discharges of interest. In all of the gas mixtures examined, dissociative electronic excitation is the major source of Cl atoms. The branching for neutral products during dissociative excitation of CCl_4 have not been measured. Kinetic studies, though, suggest that the major branching is to CCl_2+2Cl, and we have used that branching here.[10] Only a small fraction of the Cl^- produced by dissociative attachment leaves the discharge since the heavy Cl^- is trapped by the ambipolar fields. The vast majority of Cl^- is ultimately neutralized by ion–ion collisions, and so dissociative attachment also represents a volumetric source of Cl atoms.

Electron impact ionizations of HCl and Cl_2 are not dominantly dissociative whereas those for CCl_4 are dissociative. The major branching for dissociative ionization of CCl_4 is to $CCl_3^+ + Cl + e$. Therefore, to first order, ionization of HCl and Cl_2 are not sources of Cl atoms whereas ionization of CCl_4 is. HCl^+ and Cl_2^+ can, however, undergo dissociative recombination which does produce Cl atoms. At the pressures and densities of interest, this is not a particularly large source of Cl atoms. The majority of volumetric losses of positive ions result from ion–ion neutralization. These processes are generally dissociative and at high pressure are a significant source of Cl atoms. Most positive ions diffuse out of the plasma and recombine on the electrodes or walls, at least at lower pressures. The products of wall catalyzed recombination are not known since the dissociative states which are formed during the recombination process can be rapidly quenched to the ground state of the ion. For purposes of discussion, we have assumed that positive ion recombination on surfaces is not dissociative, whereas positive ion recombination in the bulk is dissociative. In any event, this process makes only minor contributions to Cl atom production. Penning and charge exchange reactions with helium excited states and ions also produce Cl atoms, though they also make only minor contributions. The fractional contributions of various processes to Cl atom production are shown in Table III. In all cases, dissociative electronic excitation is the dominant source of Cl atoms. Ionization, attachment, and neutralization processes produce only a few percent of the Cl atoms. Dissociative recombination makes only minor contributions to the production of Cl atoms.

The relative efficiencies for producing Cl atoms (production rate/power deposition) are shown in Fig. 9 for the gas mixtures studied here. The efficiencies are only weak functions of voltage and hence power deposition provided that the Cl donors are not depleted. The efficiency in-

TABLE III. Fractional contributions to Cl atom production.

Process	Gas mixture (0.25 Torr)		
	He/Cl_2 (100 V)	He/HCl (100 V)	He/CCl_4 (600 V)
Dissociative excitation	0.97	0.90	0.91
Dissociative ionization	...	...	0.04
Dissociative recombination	3.3×10^{-4}	7.0×10^{-4}	1.4×10^{-5}
Dissociative attachment	0.03	0.08	0.04
Ion–ion neutralization	2.5×10^{-3}	0.02	1.1×10^{-3}
Penning and charge exchange	...	...	9.2×10^{-3}

creases with increasing gas pressure primarily because the fractional power lost to ion bombardment of the electrodes is smaller. One might also expect the efficiency to increase with decreasing voltage for the same reason. This trend is observed for HCl and higher pressures of Cl_2. An increase in the efficiency of producing Cl atoms by dissociative excitation apparently compensates for this effect at lower pressures. Cl atom production efficiency in Cl_2 is larger than in HCl primarily because all dissociative processes yield two Cl atoms, as opposed to one. The net production efficiency for CCl_4 is surprisingly similar even though its operating voltage is much higher.

Since the emphasis of this study was on the plasma kinetics of Cl discharges we did not consider flow or depletion of the feedstock gases in the model. Clearly, in a sealed off chamber in which etching is taking place, a steady state is not achieved because Cl is being consumed by the etching process and not being replenished by flow. One can estimate the depletion of the feedstock gases in, for example, He/Cl_2 discharges in the following manner. The plasma averaged values of Cl and Cl_2 can be obtained from

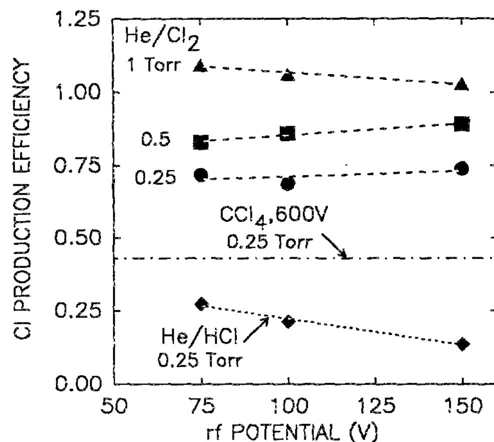

FIG. 9. Relative Cl atom production efficiency for all gas mixtures investigated.

$$\frac{d[\mathrm{Cl}]}{dt}=S-\frac{sD[\mathrm{Cl}]}{\Lambda^2}-\frac{[\mathrm{Cl}]}{\tau}, \quad (2a)$$

$$\frac{d[\mathrm{Cl_2}]}{dt}=\frac{[\mathrm{Cl_2}]_0-[\mathrm{Cl_2}]}{\tau}-\frac{S}{2}+\frac{s'D[\mathrm{Cl}]}{2\Lambda^2}, \quad (2b)$$

where S is the source of Cl atoms, D is the diffusion coefficient for Cl, Λ is the diffusion length, s is the total reactive sticking coefficient for Cl, s' is the reactive sticking coefficient for reassociation of Cl to form Cl_2, $[Cl_2]_0$ is the influx density of Cl_2, and τ is the residence time for flow. In parallel plate geometries, $\Lambda=L/2\pi$ and for our conditions $D\simeq D_0/P$, where $D_0=400$ cm^2-Torr/s and P is the gas pressure in Torr. Choosing $L=2.54$, $P=0.25-1$ Torr and $\tau\simeq0.01-0.1$ s, one can ignore flow in Eq. (2a) for $s>10^{-2}-10^{-3}$. Using this approximation, one can show that the fractional depletion of Cl_2 is

$$f=\frac{S\tau}{[\mathrm{Cl_2}]_0}(1-s'/s). \quad (3)$$

Typical values of S for plasmas sustained in $He/Cl_2=9/1$ (0.25–1 Torr) are $10^{16}-10^{17}$ $cm^3\,s^{-1}$. Using $\tau=0.03$ s, significant depletion of Cl_2 occurs at the higher source rates if $s'/s<0.5$, or if more than half the Cl removed from the plasma is by etching (as opposed to reassociation to form Cl_2).

IV. CONCLUDING REMARKS

Radio frequency discharges in He/Cl_2, He/HCl, and He/CCl_4 have been investigated using a Monte Carlo-fluid model. These gases have dramatically different electron collision transport coefficients, but produce Cl atoms by all processes with a commensurate efficiency. In all cases, dissociative electronic excitation is the dominant source of Cl atoms. Even at the low pressures investigated here, attachment in HCl mixtures is dominated by vibrationally excited HCl. The predicted electron densities are a factor of two lower when including HCl(v). For otherwise similar conditions, plasma densities are roughly twice as large in He/HCl mixtures compared to He/Cl_2 mixtures, an effect largely attributed to the lower rate of attachment to ground state species. In He/CCl_4, and to a lesser extent in He/Cl_2 mixtures, the modulation between electron sources and loss in the (z,ϕ) phase space is quite deep. This results in the steady state being maintained by a balance between two rapid processes: ionization and attachment. This mode of operation may explain the sensitivity of similar gas mixtures to small changes in operating parameters.

ACKNOWLEDGMENTS

The authors would like to thank the reviewers for helpful comments. This work was supported by the IBM East Fishkill Facility, the National Science Foundation (ECS91-09326, CTS91-13215), the Semiconductor Research Corporation, and the University of Wisconsin Engineering Research Center for Plasma Aided Manufacturing.

[a]Present address: General Electric Research and Development, P.O. Box 8, Schenectady, NY 12301.
[b]Author to whom correspondence should be addressed.

[1]D. L. Flamm in *Plasma Etching: An Introduction*, edited by D. M. Manos and D. L. Flamm (Academic, San Diego, 1989), pp. 146–155, and references therein.
[2]G. L. Rogoff, J. M. Kramer, and R. B. Piejek, Trans. Plasma Sci. **14**, 103 (1986).
[3]M. Meyyappan and T. R. Govindan, Trans. Plasma Sci. **19**, 122 (1991).
[4]S-K. Park and D. J. Economou, J. Appl. Phys. **68**, 3904 (1990).
[5]E. S. Aydil and D. J. Economou, J. Electrochem. Soc. **139**, 1396 (1992); E. S. Aydil and D. J. Economou, J. Electrochem. Soc. **139**, 1396 (1992).
[6]T. J. Sommerer and M. J. Kushner, J. Appl. Phys. **71**, 1654 (1992).
[7]Transient measurements of electron densities in rare gas and attaching gas mixtures in rf discharges using microwave interferometry do not show low frequency oscillations. K. Greenberg, Sandia National Laboratories (private communication).
[8]M. Hayashi in *Swarm Studies and Inelastic Electron-Molecule Collisions*, edited by L. C. Pitchford, B. V. McKoy, A. Chutjian, and S. Trajmar (Springer, New York, 1987), pp. 167–187.
[9]K. Leiter, K. Stephan, E. Mark, and T. D. Mark, Plasma Chem. Plasma Proc. **4**, 235 (1984).
[10]F.-W. Breitbarth and S. Rottmayer, Plasma Chem. Plasma Proc. **6**, 381 (1986).
[11]B. M. Penetrante and J. N. Bardsley, J. Appl. Phys. **54**, 6150 (1983).
[12]J. N. Bardsley and J. M. Wadhera, J. Chem. Phys. **78**, 7227 (1983).
[13]Makoto Hayashi, Nagoya Institute of Technology Report No. IPPJ-AM-19. Gokiso-cho, Showa-ku, Nagoya 466, Japan.
[14]J. P. Boeuf and E. Marode, J. Phys. D **15**, 2169 (1982).
[15]D. Rapp and P. Englander-Golden, J. Chem. Phys. **43**, 1464 (1965).
[16]L. Vriens, Phys. Lett. **8**, 260 (1964).
[17]W. C. Fon, K. A. Berrington, P. G. Burke, and A. E. Kingston, J. Phys. B **14**, 2921 (1981).
[18]M. Mitchner and Charles H. Kruger, Jr., *Partially Ionized Gases* (Wiley, New York, 1973).
[19]R. Deloche, P. Monchicourt, M. Cheret, and F. Lambert, Phys. Rev. A **13**, 1140 (1976).
[20]A. V. Phelps, Phys. Rev. **99**, 1307 (1955).
[21]S.-B. Zhu, Ph.D. thesis, University of California at San Diego, 1984.
[22]J. B. A. Mitchell, Phys. Rep. **186**, 215 (1990).
[23]C. H. Fisher, J. J. Ewing, T. E. Dehart, M. J. Kushner, and J. McDaniels, Appl. Phys. Lett. **48**, 1574 (1986).
[24]C. Gorse, M. Capitelli, R. Celiberto, R. Winkler, and J. Wilhem, J. Phys. D **23**, 1041 (1990).
[25]V. M. Donnely, D. L. Flamm, and G. Collins, J. Vac. Sci. Technol. **21**, 817 (1982).
[26]R. A. Gottscho, Phys. Rev. A **36**, 2233 (1987).
[27]M. B. Hopkins, M. Bacal, and W. G. Graham, J. Appl. Phys. **70**, 2009 (1991).